Journal of Composite Materials 50 (2016) p. 1921-1935
DOI: 10.1177/0021998315597742

# Cluster analysis of acoustic emission signals for 2D and 3D woven carbon fiber/epoxy composites

Li Li[a,b,*], Yentl Swolfs[b], Ilya Straumit[b], Xiong Yan[a], Stepan V. Lomov[b]

[a]Key Laboratory of Textile Science and Technology, Ministry of Education, College of Textiles, Donghua University, Shanghai 201600, China

[b]Department of Materials Engineering, KU Leuven, Kasteelpark Arenberg 44, B-3001 Leuven, Belgium

*Corresponding author: lililainey@gmail.com

## Abstract

Understanding the failure mechanisms in textile composites based on acoustic emission (AE) signals is a challenging task. In the present work, unsupervised cluster analysis is performed on the AE data registered during tensile tests on 2D and 3D woven carbon fiber/epoxy composites. The analysis is based on the k-means++ algorithm and principal component analysis. Peak amplitude and frequency features – peak frequency for 2D woven composites and frequency centroid for 3D woven composites – were found to be dominant in cluster analysis. Cluster bounds were identified for both reinforcement types. These bounds do not differ for both reinforcement types and can be used as a starting point for AE analysis of other carbon fiber/epoxy composites. The statistics of high frequency AE events are compared with the estimates obtained from a fiber bundle model based on Weibull fiber strength statistics. The number of AE events agrees well with the number of groups of carbon fibers that fail simultaneously. This finding may provide a new way to explain why the Weibull distribution predicts much more fiber breaks than measured by AE.

**Keywords:** A. Polymer-matrix composites; A. 3-Dimensional reinforcement; A. Carbon fiber; D. Acoustic emission

# 1. Introduction

Acoustic emission (AE) registration is an important non-destructive technique for detecting and identifying damage development in fiber-reinforced composites[1-7]. The AE technique has been extensively applied to carbon fiber reinforced polymers (CFRP)[1-5], allowing identification of damage initiation and propagation during loading. A crucial but unresolved problem is the development of methods for identifying damage modes based on the parameters of AE events, such as amplitude, frequency and signal rise time. The evolution of cumulative energy of AE events has been used for identifying damage initiation and propagation thresholds in textile composites[3, 4, 8]. However, this approach does not allow identification of the damage modes associated with the AE events.

Journal of Composite Materials 50 (2016) p. 1921-1935
DOI: 10.1177/0021998315597742

Cluster analysis is a powerful methodology to analyze multi-parametrical AE signals[9-11]. This analysis classifies events based on clustering of their multi-parametrical descriptors. This hence creates a framework for subsequent identification of the links between the established cluster event classification and the physical nature of the damage.

Classifications of AE events based on amplitude have been performed in the past for unidirectional and cross-ply CFRP laminates[12, 13]. Peak amplitude alone does not seem to be a reliable parameter to distinguish damage mechanisms. Valentin et al.[12] and Liu et al.[13] concluded that matrix cracking was associated with low amplitude signals, fiber-matrix debonding with medium amplitude events, and fiber failure with high amplitude events. This classification contradicts the one proposed by Berthelot et al.[14], which suggests that high amplitude signals correspond to matrix cracking, while low amplitude signals correspond to fiber breakage.

Cluster analysis based on both time and frequency features showed that the peak frequency of an AE signal can represent specific damage mechanisms[11, 15]. The low frequency range is normally attributed to matrix cracking, while high frequency is attributed to fiber breakage. In contrast, the frequency range for delamination and fiber-matrix debonding varies in different studies. De Groot et al.[15] and Gutkin et al.[11] investigated carbon/epoxy laminates in different tests and obtained similar frequency bands for the fiber-matrix debonding (medium frequency range from 200 to 300 kHz) and fiber breakage (high frequency over 300 kHz). However, these authors mention different frequency ranges for the other damage modes. Matrix cracking was related to the 50-180 kHz frequency range in De Groot et al.[15], whereas this range was below 50 kHz in Gutkin et al.[11]. Fiber pull-out corresponded to frequencies around 200 kHz in De Groot et al.[15] but to frequencies above 500 kHz in Gutkin et al.[11]. Delamination-related AE events corresponded to a higher frequency range: from 220 to 300 kHz in De Groot et al.[15], compared to 50 to 150 kHz in Gutkin et al.[11].

Sause et al.[10] identified clusters of AE signals for unidirectional glass fiber reinforced polymers (GFRP) and CFRP composites using the approach proposed in literature[9]. They found that frequency features can help to distinguish between matrix cracking, interfacial failure and fiber breakage. Accumulated AE signal amplitudes also reflected the extent of the damage, while the frequency feature identified the damage mechanism[10]. The works cited above all deal with unidirectional or 2D woven laminates. Cluster analysis of AE signals applied to 3D woven CFRP has not been performed yet.

In our previous study[5], the applicability of the AE frequency bands proposed in literature[11, 15] was investigated for 3D carbon/epoxy non-crimp woven composites. The number of high frequency AE events was found to be inconsistent with the number of fiber breaks predicted from simple Weibull statistics for fiber strength. However, the findings in literature[5] are not fully conclusive for three reasons. Firstly, the observed inconsistency was supposedly attributed to the presence of random individual fiber waviness within the yarns. This can change the fiber breakage conditions, but was not further investigated. Secondly, the statistics of multiple fiber

breakage were not considered. Thirdly, the authors did not perform a full cluster analysis, and may not have been able to fully distinguish all AE signals.

The present paper deals with these deficiencies. A cluster analysis is performed on the measurements in literature[3, 4]. The analysis of the fiber breakage statistics is extended to include fiber misalignment and collective fiber breakage[16-20]. The AE analysis methodology that was previously used for 2D and 3D glass/epoxy woven composites[21], is now applied to 2D and 3D carbon fiber-reinforced woven composites[3, 4]. The internal architecture of these reinforcements is comparable to that of their glass fiber counterparts in literature[21]. This study has two objectives. The first objective is to find out whether AE events in carbon/epoxy woven composites can be represented with the same cluster construction as for their glass/epoxy counterparts. This includes establishing generic cluster bounds for 2D and 3D composites, as was done for glass/epoxy composites in literature[21]. The second objective is to refine the statistics of fiber breakage in 2D and 3D woven composites based on more detailed analysis compared to literature[5]. This analysis investigates the influence of fiber misalignment and collective fiber breakage in fiber bundles. Comparing the fiber break statistics with the high frequency clusters provides additional grounds for identifying these clusters with fiber breakage.

Signal attenuation and wave propagation in general (for example, the specimen transfer function) can have an influence on the damage identification, but these effects were not studied by us. In a recent paper [22] these effects are investigated in detail and will be an important component of AE analysis in the future work.

# 2. Materials and methods

## *2.1 Materials and test methods*

The materials used in this study are carbon fiber/epoxy composites based on balanced 2D twill 2/2 and 3D non-crimp orthogonal woven composites, which were manufactured by resin transfer molding and vacuum assisted resin infiltration.This was performed at a vacuum pressure of ~0.1MPa in the similar condition and have similar fiber volume fraction and thickness. Their internal structure, experimental procedure and mechanical behavior were previously described in detail[3,4]. The structure and properties of the preforms and composites are shown in Fig. 1 and Table 1[3, 4]. Fig 1 also shows typical crack patterns in the studied materials. Tensile tests were performed according to ASTM D3039 standard. All specimens were 250 mm long with a gauge length of 170 mm. The nominal width of the 2D and 3D specimens was 25 mm and 31 mm, respectively. The surface strain was measured using a digital image correlation system. The 2D twill specimens were tested only in the warp direction, as the weave was balanced. The 3D specimens were tested both in warp and fill direction, as this weave was not balanced. The reader can refer to literature[3,4] for detailed information on the materials, specimens and test methods, as well as for detailed description of the damage development, including images of the cracks.

Journal of Composite Materials 50 (2016) p. 1921-1935
DOI: 10.1177/0021998315597742

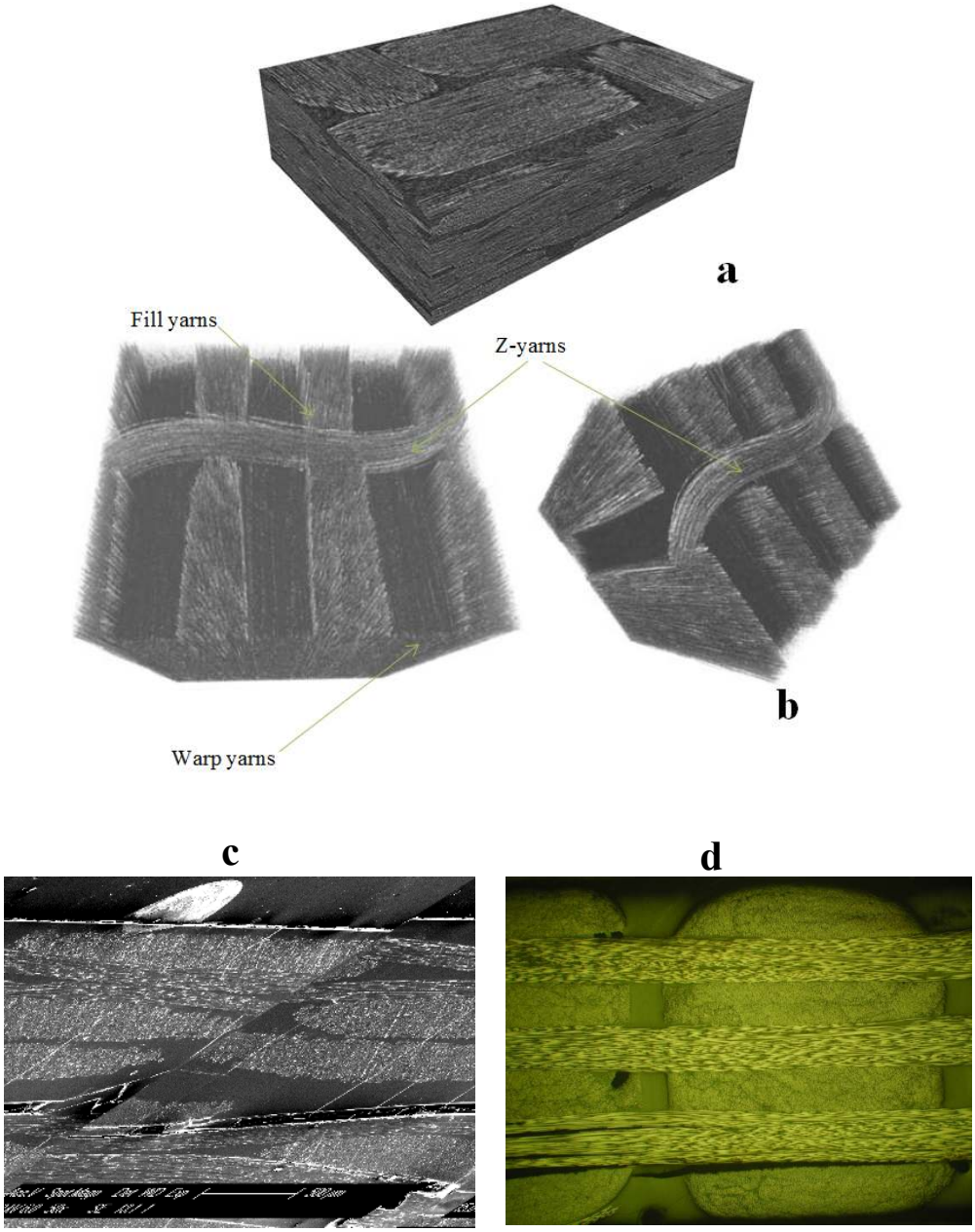


**Fig. 1: MicroCT images of the reinforcement architecture of (a) the 2D twill 2/2 woven fabric[3], and (b) the 3D non-crimp orthogonal woven fabric[4,5], and typical crack patterns in the 2D (c) and 3D (d) specimens under warp-direction loading.**

**Table 1: Properties of the preforms and the carbon/epoxy composites: 2D[3] and 3D[4].**

| | | 3D non-crimp | 2D twill 2/2 |
|---|---|---|---|
| | Fabric plies | 1 | 7 (warp direction in all plies coincides) |
| | Areal density (g/m$^2$) | 2499 | 300 |
| Warp | Yarn density (ends/cm) | 4,72 | 3,5 |
| | Carbon yarn | Toho Tenax 12 K, 800 tex, | AS4C GP 6K, 400 tex |

Journal of Composite Materials 50 (2016) p. 1921-1935
DOI: 10.1177/0021998315597742

| | | | | |
|---|---|---|---|---|
| Preforms | | Fiber volume fraction (%) | 46,12 | _ |
| | Fill | Insertion density (picks/cm) | 3.91 | 3,5 |
| | | Carbon yarn | Toho Tenax 12 K, 800 tex | AS4C GP 6K, 400 tex |
| | | Fiber volume ratio (%) | 51,24 | _ |
| | Z yarns | Yarns (tex) | Toho Tenax 1 K, 66 tex | _ |
| | | Fiber volume ratio (%) | 2.64 | _ |
| Composites | | Fiber volume fraction (%) | 51.1 | 55.2 |
| | | Thickness(mm) | 2.76 | 2.14 |
| | | Resin | Epikote 828 LVEL hardener: Dytek DCH-99 | West System 105 epoxy hardener: 209 Extra Slow Hardener |

The AE events were monitored by Vallen AMSY-5 system with the sensors being 120 mm apart. The preamplifier used was AEP4 with threshold 34 dB. The transducers used were Digital Wave B-1025 and it can be used in a temperature range of -50 °C to 100 °C[4,5]. The transfer function of this sensor is illustrated in Fig. 2[23]. The acquisition parameters are summarized in Table 2[3,4]. The linear location is used in this study from two sensors mounted on the tensile specimens, and calculated by Vallen AE software. The AE data of 2D and 3D carbon/epoxy woven specimens recorded in the previously reported experiments[3,4] was employed in this work. Previous studies have identified the following damage types during the tensile loading by optical microscopy[3-5]:

- for the 2D woven composites: matrix cracking, including transverse and later longitudinal cracks in the yarns, and local delamination;

- for the 3D woven composites: cracks in the z-yarns and at its boundaries as well as transverse and longitudinal cracks[4,5].

The cluster analysis of AE events should reflect the differences between these damage types and discriminate between them. Three tests for each specimen type were chosen for cluster analysis in this study. The specimens are referred to as 2D-n, 3DW-n, 3DF-n, where ‘2D’ and ‘3D’ indicates the type of preform, ‘W’ and ‘F’ indicates the warp and fill direction for 3D composites respectively, and $n$ = 1,2,3 is the specimen number.

**Table 2: Data acquisition parameters of the acoustic emission test[3-5].**

| | |
|---|---|
| Software | Vallen AMSY-5 |
| Amplifiers | Vallen AEP4 |
| Amplification, dB | 34 |
| Discrimination time, | 0.4 |
| Rearm time, ms | 3.2 |
| Range, MHz | 0.025–1.6 |
| Sample rate, MHz | 5 |

Journal of Composite Materials 50 (2016) p. 1921-1935
DOI: 10.1177/0021998315597742

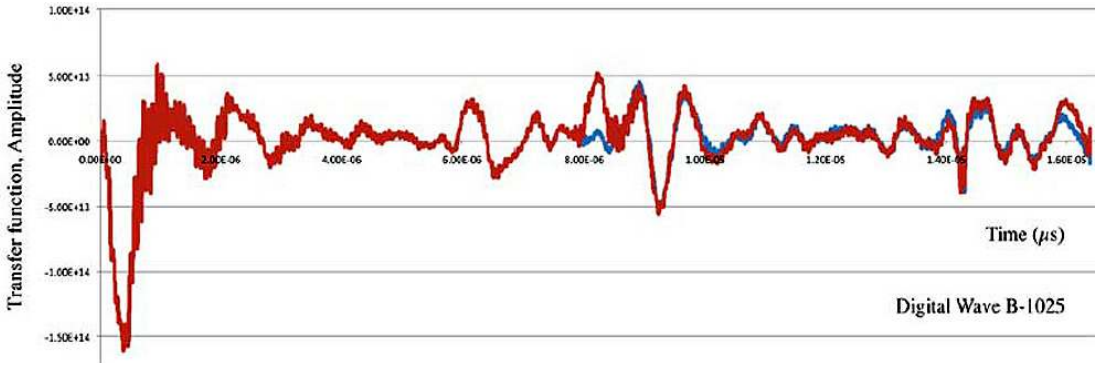


**Fig. 2: Transfer function of Digital Wave B-1025 sensor[23].**

## 2.2 Cluster analysis methods

The same cluster analysis was performed on AE events of 2D and 3D carbon/epoxy composites as it was performed for 2D and 3D glass/epoxy composites. The details of the employed analysis can be found in literature[21]. The carbon/epoxy composites studied here, have the same 3D weave pattern as the glass/epoxy composites in literature[21].

Nine AE signal features were considered in this paper, which are signal peak amplitude, duration, rise time, energy, counts, RA value, peak frequency, frequency centroid and weighted frequency. The definition of time domain parameters peak amplitude, duration, rise time and counts are presented in Fig. 3a. Peak frequency is the component of the signal frequency spectrum with the highest Fast Fourier transform magnitude. The frequency centroid of gravity, or frequency centroid, is defined as:

$$F_{CoG} = \frac{\int f \cdot A(f)df}{\int A(f)df}, \tag{1}$$

where $f$ is the frequency in the spectrum, $A(f)$ is the magnitude of the corresponding frequency from the Fourier transformation of the signal, with unit mV [9]. The definition of these two frequency parameters is illustrated in Fig. 3b.

Journal of Composite Materials 50 (2016) p. 1921-1935
DOI: 10.1177/0021998315597742

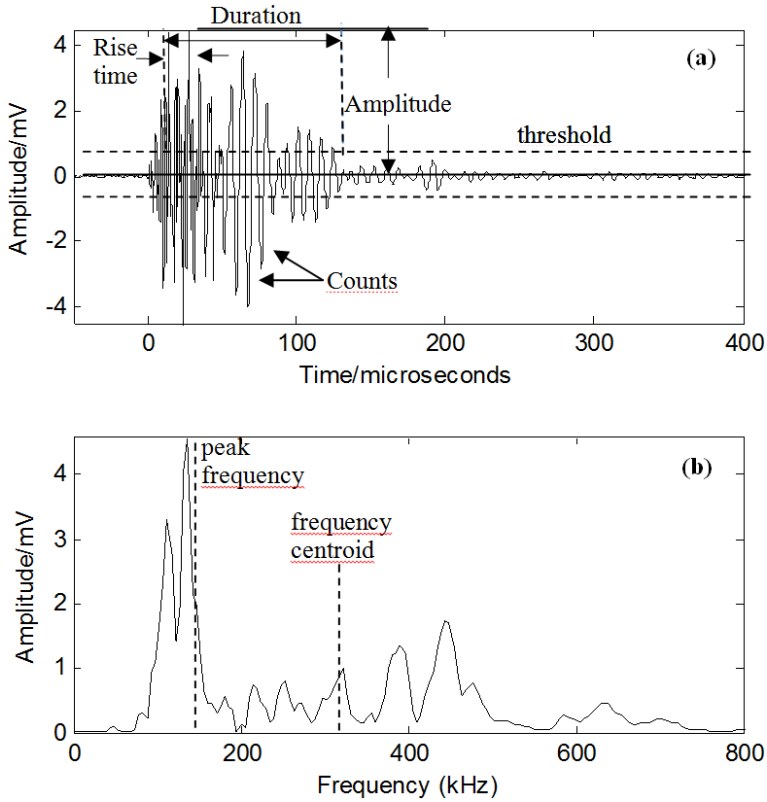


**Fig. 3: The spectrum of a typical AE signal: (a) time domain, (b) frequency spectrum after Fast Fourier Transform, and AE frequency features - peak frequency and frequency centroid.**

Four parameters were chosen as AE descriptors out of these nine AE features by feature selection procedure. This procedure is based on the so-called Laplacian score[24], which is based on the proximity of the data classes in a multi-parametrical space. This score has also been used in literature[21]. It ranges between 0 and 1, where a larger score indicates a higher cluster ability of the investigated feature. This procedure deduced four AE parameters that should be used in the cluster analysis: peak amplitude (PA), peak frequency (PF), rise time divided by peak amplitude (RA value) and frequency centroid of gravity (FCoG).

Principal Component Analysis (PCA) and k-means++ algorithm were used to cluster the AE events. The Silhouette Coefficient (SC) and Davies-Bouldin index (DB) were used to evaluate the cluster validity, with a higher SC and lower DB indicating better cluster quality. The reader can refer to Li et al.[21] for the details of the employed algorithms. The cluster analysis is performed using the Statistics toolbox in MatLab R2013a.

# 3. Cluster analysis results and discussion

## *3.1 Repeatability of AE registration*

Before performing the cluster analysis, the repeatability of the AE events for different tests was investigated to ensure consistency of the AE data. Fig. 4 shows the AE

Journal of Composite Materials 50 (2016) p. 1921-1935
DOI: 10.1177/0021998315597742

energy as a function of the applied strain for all individual tests on the 2D and 3D specimens. Fig. 5 represents the peak amplitude and peak frequency distribution for all the tests. For all the 2D and 3D woven composites, the peak amplitude distribution and peak frequency distribution follow a similar pattern. They have fewer events in the amplitude range over 55 dB and frequency range over 65 kHz, compared to the low amplitude and the low frequency range. It can be concluded from the data in Fig. 4 and Fig. 5 that the repeatability of AE registration is satisfactory and that cluster analysis can be performed with confidence.

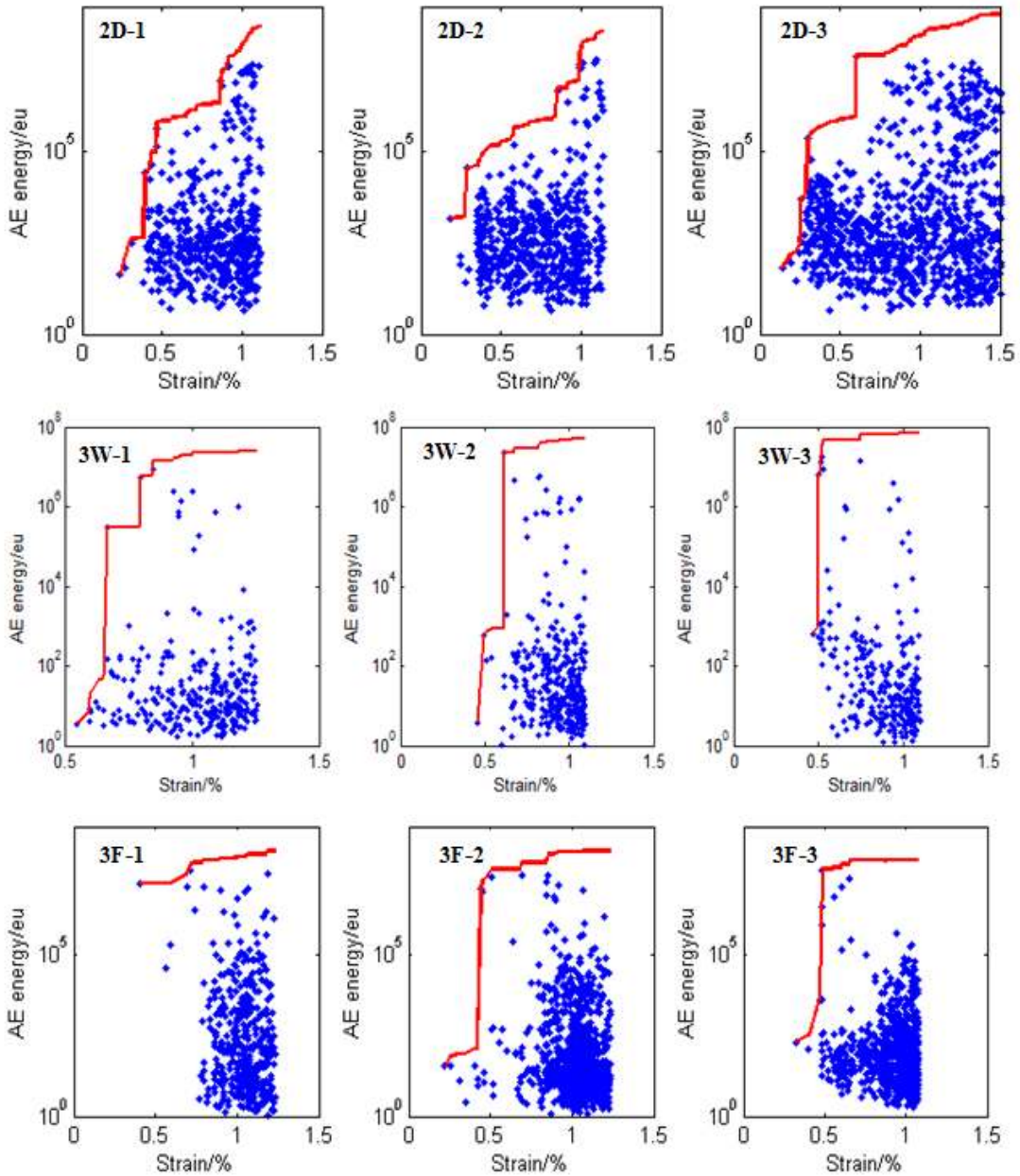


**Fig. 4: AE event patterns for all 2D and 3D individual tests. Blue dots represent the energy of AE events, while the red line represents the cumulative AE energy.**

Journal of Composite Materials 50 (2016) p. 1921-1935
DOI: 10.1177/0021998315597742

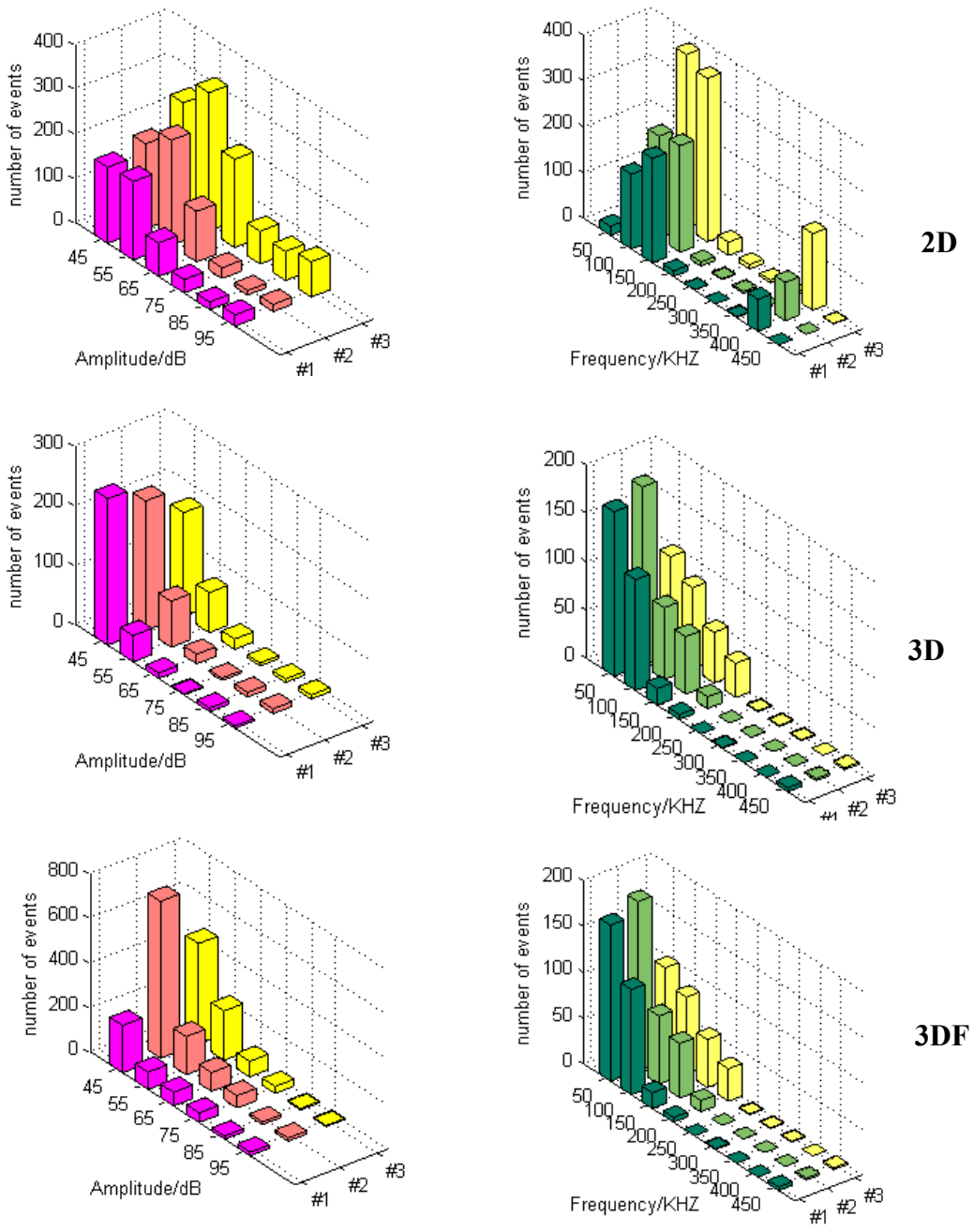


**Fig. 5: Distribution of peak amplitude and peak frequency of the AE events for the individual tests of 2D, 3D-warp (3DW) and 3D-fill (3DF) specimens.**

## *3.2 Definition of the clusters*

Principle component analysis (PCA) is an orthogonal linear transformation method. It transforms multidimensional AE data into a set of linearly uncorrelated features in a new coordinate system, which is based on the covariance matrix of the dataset. These

Journal of Composite Materials 50 (2016) p. 1921-1935
DOI: 10.1177/0021998315597742

new features called principal components have the maximum variance amongst all possible transformations of the original coordinate system[25].

The variance percentage and cumulative variance of each principal AE component for representative samples are shown in Fig. 6a. The first two principal components can explain more than two-thirds of the total variance, meaning that the two components can visualize the AE data. This is confirmed by Fig. 7, in which clusters are well separated by the projection onto the first two principal components. For different specimen types, the main AE features corresponding to the first two principal components vary, which can be seen from the coefficients of the principal components in Table 3. The principal components *Pdi*, *i=1…4*, which are defined by the principle component analysis (PCA) algorithm are expressed as:

$$Pdi = \lambda_1 PA + \lambda_2 PF + \lambda_3 RA + \lambda_4 FCoG, \quad i = 1...4 \tag{2}$$

where $\lambda_i$ are the principal components coefficients. The coefficients for different specimens are summarized in Table 3, while the contributions of the four AE parameters to the principal components are shown in Fig. 6b. For 2D specimens, the largest coefficient in the first principal component is the first element, corresponding to the peak amplitude (PA). The second principal component is the peak frequency (PF). The coefficient of the second element, related to the peak frequency, is only slightly lower than the third one (RA value). PF was chosen as the second principal component based on its stronger cluster ability reflected by its high Laplacian score. This score is 0.97 for PF, but only 0.66 for RA. Therefore, peak amplitude and peak frequency can represent Pd1 and Pd2 respectively for 2D samples. The same analysis of the coefficients leads to the conclusion that for 3D samples tested both in warp and fill direction, the peak amplitude and frequency centroid are important for Pd1 and Pd2. This is evidenced from the clear separation of the AE events by the corresponding AE parameters for 2D and 3D specimens (see Fig. 8).

Journal of Composite Materials 50 (2016) p. 1921-1935
DOI: 10.1177/0021998315597742

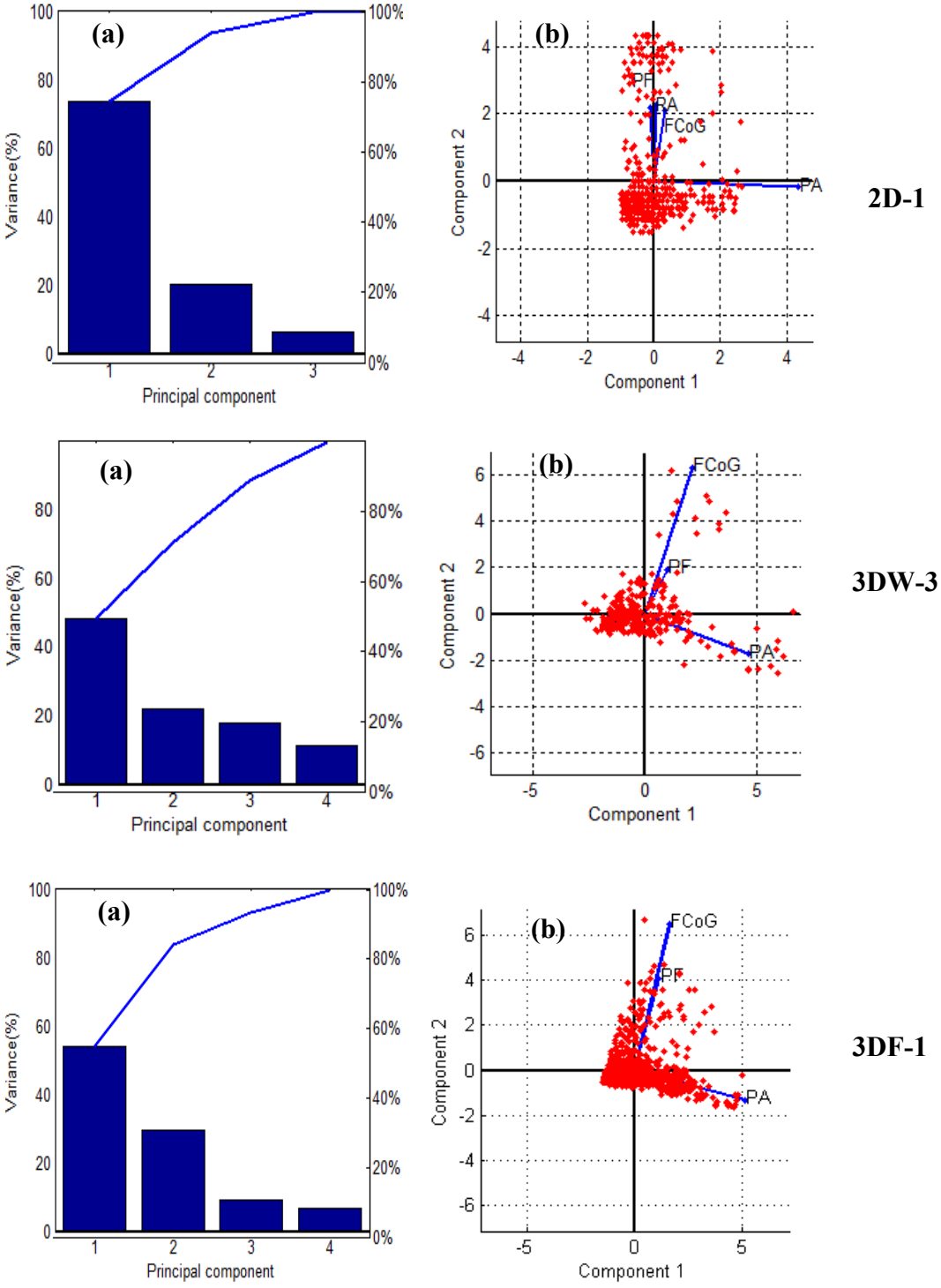


**Fig. 6: (a) Variance (bars) and cumulative variance (line) of each principal component for representative samples and (b) component coefficients of AE parameters for the first two principal components.**

Journal of Composite Materials 50 (2016) p. 1921-1935
DOI: 10.1177/0021998315597742

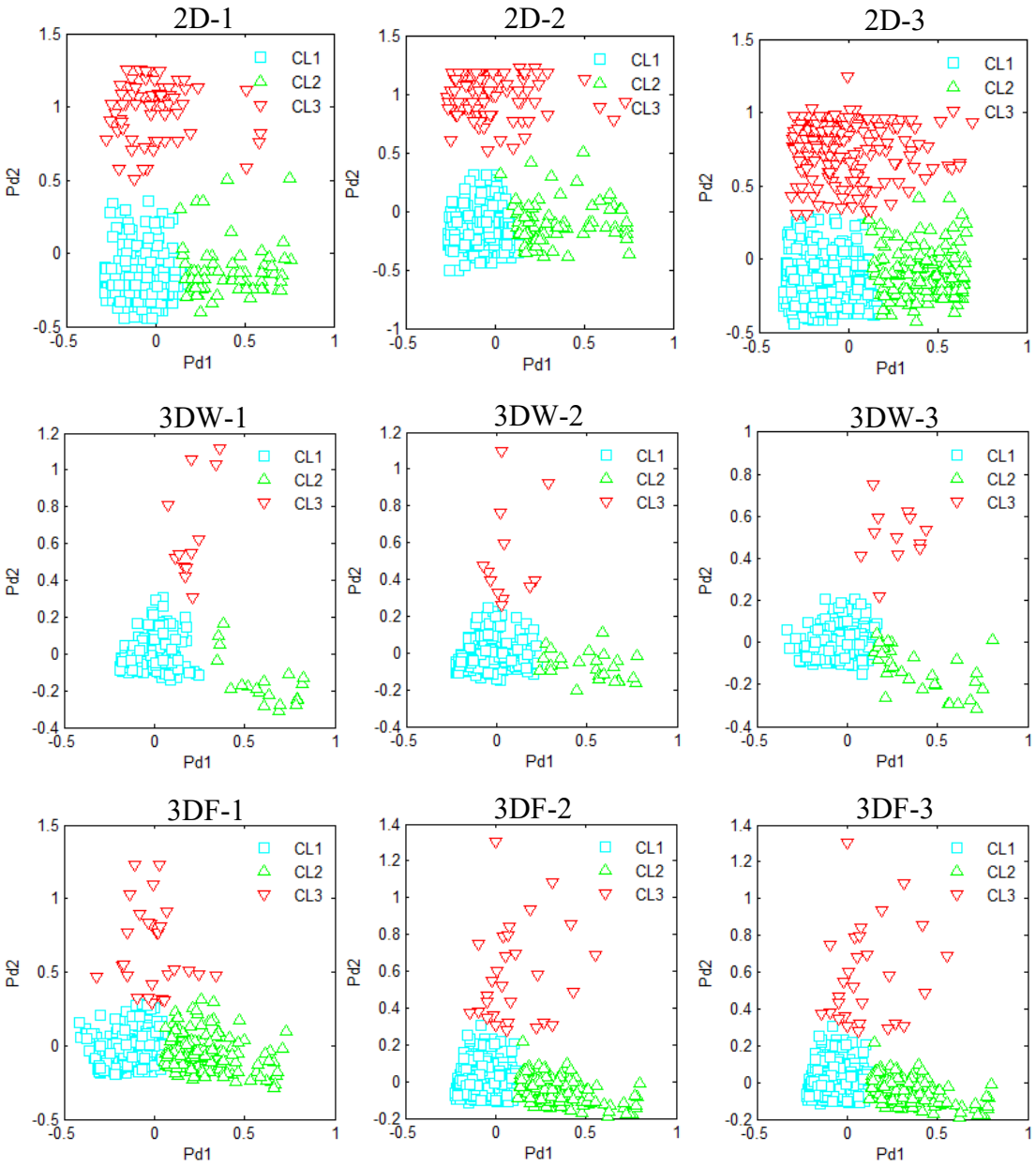


**Fig. 7: PCA projection of k-means ++ clustering of the AE events of textile composites to three clusters by the selected AE features.**

**Table 3 The principal component coefficients for four AE parameters: peak amplitude, peak frequency, RA value and frequency centroid.**

| | 2D | | 3DW | | 3DF | |
|---|---|---|---|---|---|---|
| | Pd1 | Pd2 | Pd1 | Pd2 | Pd1 | Pd2 |
| λ1 | **4.34** | -0.17 | **4.66** | -1.75 | **5.12** | -1.32 |
| λ2 | -0.10 | **2.17** | 1.00 | 1.92 | 1.13 | 4.08 |
| λ3 | 0.06 | 2.24 | -1.75 | -0.34 | -0.88 | -0.48 |
| λ4 | 0.33 | 2.09 | 2.14 | **6.31** | 1.63 | **6.49** |

Journal of Composite Materials 50 (2016) p. 1921-1935
DOI: 10.1177/0021998315597742

Fig. 8 shows the three clusters separated by the amplitude and frequency features, referred to as CL1, CL2 and CL3. The validity of the clusters is can be seen from the Silhouette value and Davies-Bouldin's index in Table 4. For 2D specimens, three clusters are separated by the peak amplitude and peak frequency. CL1 has a low peak amplitude and low peak frequency, in the range of 30-70 dB and 0-300 kHz. CL2 has a high peak amplitude of above 70 dB and low peak frequency with the same range as CL1. CL3 has broad peak amplitude range from 40 dB to 100 dB and a high peak frequency, above 300 kHz.

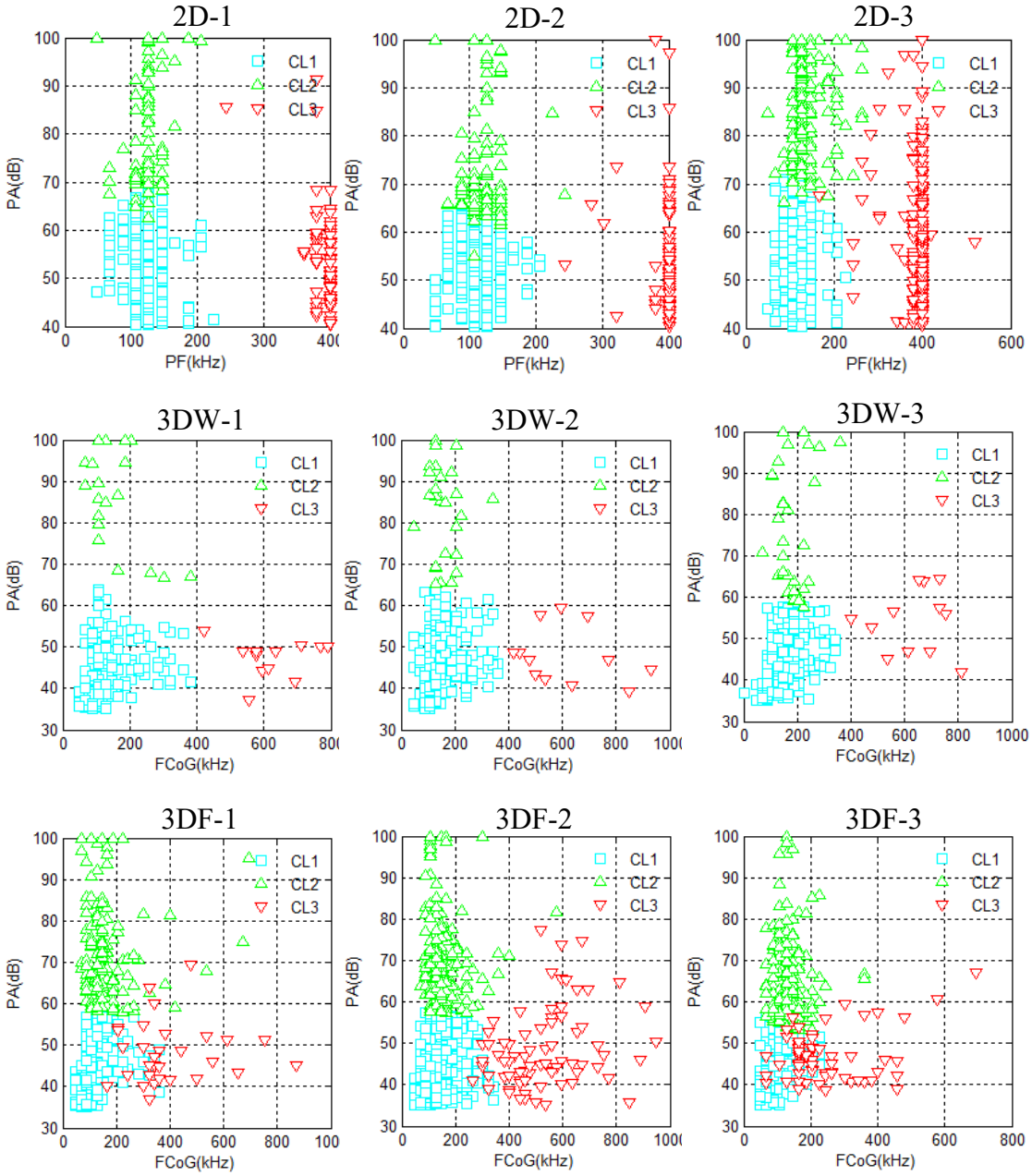


**Fig. 8: Cluster results separated by peak amplitude as a function of frequency of the AE events for**

**all analyzed specimens to three clusters by the selected AE features and k-mean++ algorithm.**

**Table 4: Three groups clustered by k-means++ for all specimens. The SC and DB-index prove the cluster validity.**

| Samples | Number of events | *SC* | D-B index | Percentage of events in each cluster | | |
|---|---|---|---|---|---|---|
| | | | | CL1 | CL2 | CL3 |
| 2D-1 | 519 | 0.71 | 0.75 | 0.71 | 0.15 | 0.14 |
| 2D-2 | 588 | 0.64 | 0.84 | 0.76 | 0.15 | 0.07 |
| 2D-3 | 588 | 0.72 | 0.69 | 0.62 | 0.19 | 0.19 |
| 3DW-1 | 310 | 0.87 | 0.74 | 0.89 | 0.06 | 0.05 |
| 3DW-2 | 330 | 0.81 | 0.87 | 0.88 | 0.08 | 0.04 |
| 3DW-3 | 275 | 0.66 | 0.92 | 0.81 | 0.14 | 0.04 |
| 3DF-1 | 422 | 0.63 | 1.17 | 0.57 | 0.35 | 0.07 |
| 3DF-2 | 1035 | 0.73 | 0.97 | 0.75 | 0.17 | 0.08 |
| 3DF-3 | 778 | 0.58 | 1.26 | 0.71 | 0.26 | 0.03 |

For 3D woven specimens in warp direction (3DW), the three clusters are separated by the peak amplitude and frequency centroid. These clusters have the same structure as for the 2D samples: three clusters representing AE events with low amplitude – low frequency; high amplitude – low frequency, and high frequency (irrespective of amplitude). CL1 has a peak amplitude of 30-60 dB and a frequency of 0-400 kHz. CL2 has a higher peak amplitude and a lower frequency compared to CL1. The frequency range of CL3 is above 400 kHz.

For 3D woven specimens in fill direction (3DF), there is an overlap of the three clusters, especially for CL1 and CL3. On the whole, CL1 and CL2 have the same cluster distribution as 3DW: the peak amplitude range and frequency range is 30-60 dB and 0-400 kHz for CL1, while it is 55-100 dB and 0-400 kHz for CL2. CL3 on the other hand has a broad range of amplitude and frequency, 30-90 dB and above 400 kHz, and there is an overlap in the frequency from 200 kHz to 400 kHz for CL1 and CL3.

The clusters CL1-CL3 are labelled as CL-AlFl, CL-AhFl and CL-AbFh to facilitate distinguishing and discussing the clusters for all 2D and 3D composites. ‘l’, ‘h’, ‘b’ are short for “low”, “high” and “broad” respectively. ‘A’ relates to peak amplitude and ‘F’ corresponds to frequency features. CL-AlFl therefore represents a cluster with a low amplitude and low frequency, where frequency can either represent PF or FCoG. CL-AhFl represents a cluster with a high amplitude and low frequency, whereas CL-AbFh stands for broad amplitude and high frequency.

## *3.3 Discussion of the cluster analysis results*

The clusters for both 2D and 3D carbon/epoxy composites are summarized in Table 5. For 2D specimens, CL-AlFl has peak amplitudes below 70 dB, and peak frequencies below 300 kHz. The CL-AhFl peak amplitude is above 70 dB. CL-AbFh has a broad peak amplitude ranging from 30 dB to 90 dB, and a peak frequency above 300 kHz.

Journal of Composite Materials 50 (2016) p. 1921-1935
DOI: 10.1177/0021998315597742

For the 3D specimens, CL-AlFl has a peak amplitude below 60±5 dB, and a frequency centroid below 400 kHz. CL-AhFl has a peak amplitude above 60±5 dB, whereas CL-AbFh has a frequency centroid of above 400 kHz and 30-90 dB peak amplitude. Therefore, the cluster bounds for 2D are a peak amplitude of 70 dB and a peak frequency of 300 kHz. For 3D, these bounds are a peak amplitude of 60±5 dB, and a frequency centroid of 400 kHz.

**Table 5: Summary of the three clusters for 2D and 3D carbon/epoxy specimens.**

| Clusters | 2D carbon/epoxy | | 3D carbon/epoxy | | 2D&3D glass/epoxy[21] | |
|---|---|---|---|---|---|---|
| | PA (dB) | PF (kHz) | PA (dB) | FCoG (kHz) | PA (dB) | PF (kHz) |
| CL-AlFl | ≤ 70 | < 300 | < 60 ±5 | < 400 | ≤ 60 | ≤ 150 |
| CL-AhFl | > **70** | < **300** | > **60±5** | < **400** | >**60** | ≤ **150** |
| CL-AbFh | 30…90 | ≥ 300 | 30… 90 | ≥ 400 | 35…90 | > 150 |

For the 2D and 3D carbon/epoxy composites, AE events are classified by either peak frequency or frequency centroid. In the 2D specimens, transverse matrix cracks dominate the initiation and propagation of damage, leading to appearance of local delaminations between the woven plies (see Fig. 1c) [3]. In the 3D specimens the damage starts in the form of boundary cracks and Z-yarn cracks, whith further development of local debondings between the warp and weft yarns (see Fig. 1d) [4]. It is possible that this difference in damage morphology causes the different AE features in the clusters. One can speculate that relatively large interlayer delaminations in 2D specimens, which are larger than debondings between warp and weft in 3D specimens, can be expected to produce AE events with larger amplitude.

Table 5 compares cluster bounds for 2D and 3D composites reinforced with glass fibers[21] and carbon fibers. The cluster bounds of 2D and 3D glass/epoxy are a peak amplitude of 60 dB and a peak frequency of 150 kHz. 2D twill 2/2 carbon/epoxy composites have higher cluster bounds, peak amplitude with 70 dB and peak frequency with 300 kHz, compared to 2D and 3D glass/epoxy. For 3D carbon/epoxy specimens, the cluster bound of peak amplitude is similar with glass/epoxy, but the frequency bound is 400 kHz, which is higher than that of glass/epoxy with 150 kHz.

To summarize, the cluster bounds of amplitude and frequency for carbon fiber reinforced composites are higher than the ones for the glass/epoxy composites. A possible explanation is the higher stiffness of carbon fiber, which may lead to a higher amplitude and frequency of the AE signals.

Different frequency descriptors can be found for the different studied composites. Considering the signal amplitude and frequency separately does not guarantee distinct boundaries between the event groups. Therefore, it is advisable to perform a full cluster analysis to achieve a reliable classification of the AE events.

Typical signals for the three clusters for 2D and 3D carbon/epoxy composites are shown in Fig. 9. The signal spectrum shows that 2D specimens have broad frequency range for the first two clusters: CL-AlFl and CL-AhFl. The difference of the two

Journal of Composite Materials 50 (2016) p. 1921-1935
DOI: 10.1177/0021998315597742

clusters is that only the energy of CL-AhFl is higher than CL-AlFl. 3DW and 3DF specimens have similar acoustic emission signal spectrums for the three clusters. But CL-AlFl of 3D specimens has a broad frequency range, whereas events in CL-AhFl of 3D specimens are mainly in the frequency range of 0-200 kHz. For the third cluster CL-AbFh, the peak frequency is above 400 kHz for 2D. In the spectrum for 3D, it can be seen that the ratio of FFT magnitude to maximum magnitude is higher than that of CL-AhFl for frequencies above 200 kHz.

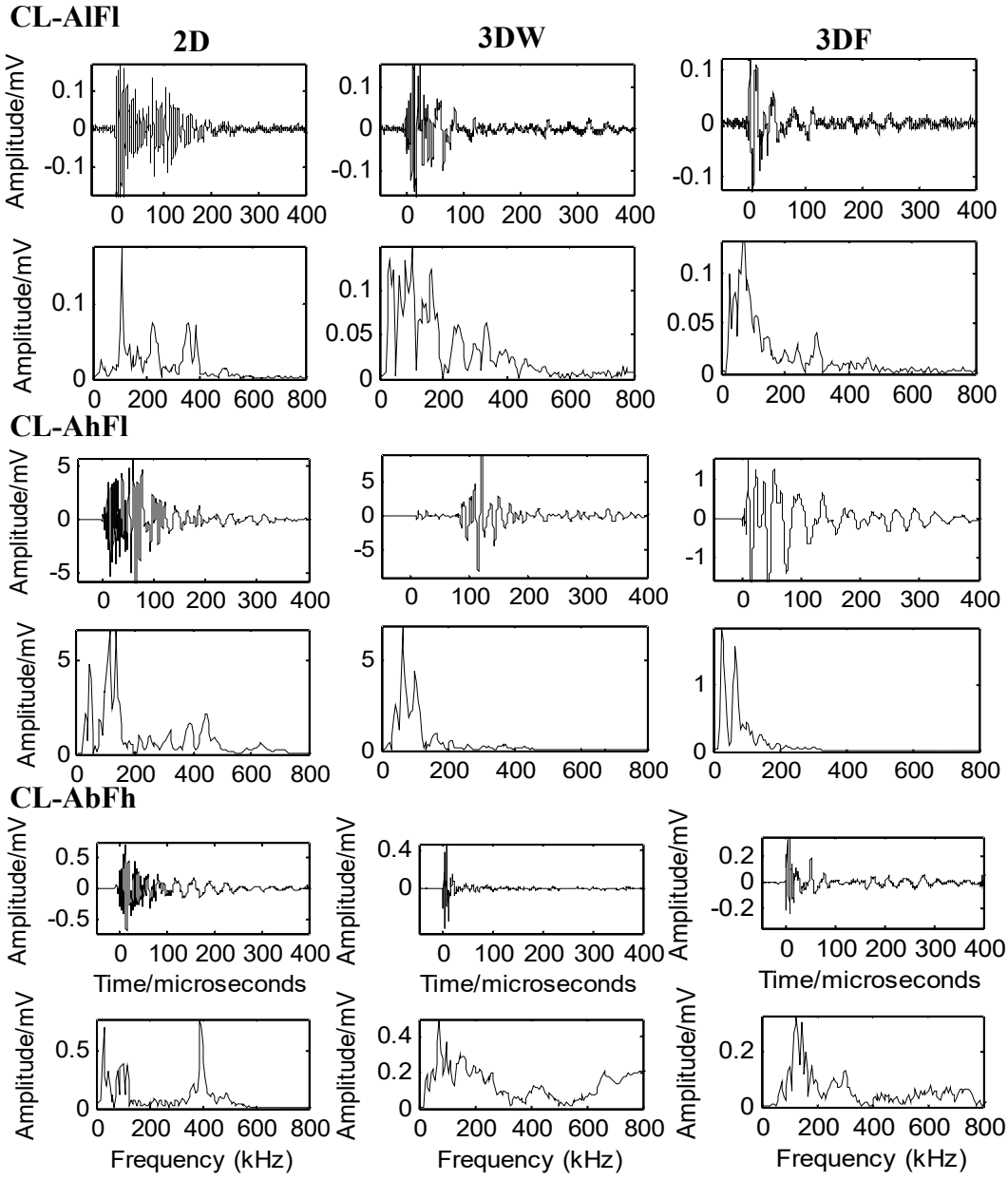


**Fig. 9: Typical AE signals and corresponding frequency spectrums for three clusters CL-AlFl, CL-AhFl and CL-AbFh for 2D, 3DW and 3DF carbon/epoxy composites.**

Journal of Composite Materials 50 (2016) p. 1921-1935
DOI: 10.1177/0021998315597742

# 4. High frequency events (CL-AbFh) and statistics of the fiber failure

The yarns in the studied composite materials have a low crimp: below 1% in the 2D woven laminates[3] and even below 0.1% in the 3D non-crimp orthogonally woven fabrics[26]. The fiber failure is therefore controlled by the strain applied to the composite. This creates the possibility to compare the statistics of the fiber failure with the number of AE events in the high frequency cluster CL-AbFh. If such a comparison shows significant similarities, then it can be considered as a validation of the connection of the high frequency AE events with fiber failure. This connection is generally accepted in literature[11, 27]. However, a preliminary Weibull-based estimation[5] has shown large discrepancies between the predicted number of fiber breaks and the number of registered high frequency AE events. Weibull estimations of the probability of individual fiber breakage indicated a much earlier start and much larger number of fiber breaks than the measurements from AE events. Here, two possible hypotheses are explored, which may resolve this discrepancy: (1) influence of the fiber misalignment on their breakage and (2) simultaneous fiber breakage in a bundle.

## *4.1 Misalignment of the fibers*

Misalignment of the fibers in the yarns / fiber bundles was estimated using a structure tensor analysis[28] of micro-CT images of the composites, shown in Fig.1. The misalignment angle of the fibers (difference between the direction of the fiber and the direction of the center line of the yarn) was found to follow a Gaussian distribution, with an average of 0 and standard deviation of 2.5°. Simple geometrical considerations relate the strain in the fiber $\varepsilon_f$, inclined by an angle $\theta$, to the elongation of the yarn $\varepsilon$ as the following equation:

$$\varepsilon_f(\varepsilon,\theta) = \max\left(0, \frac{\sqrt{(1+\varepsilon)^2 + \nu^2 tg^2\theta} - \sqrt{1+tg^2\theta}}{\sqrt{1+tg^2\theta}}\right), \quad (3)$$

where $\nu$ is Poisson coefficient of the impregnated yarn, estimated as $\nu$ =0.4. Then, the number of broken fibers $N$ in a bundle under tensile strain $\varepsilon$ can be estimated as:

$$N(\varepsilon) = N_\Sigma \int_0^\pi \psi(\theta) P(\varepsilon_f(\varepsilon,\theta)) d\theta, \quad (4)$$

where $N_\Sigma$ is the total number of fibers in the bundle, $\psi(\theta)$ is the distribution of the misalignment angles $\theta$, $P(\varepsilon_f)$ is the probability of the fiber breakage defined by Weibull distribution.

This analysis found only a negligible effect of the misalignment on the number of fiber breaks, compared to the case without misalignment (assuming $\psi(\theta) = \delta(\theta)$). After the misalignment was taken into account, the estimation of the number of broken fibers

Journal of Composite Materials 50 (2016) p. 1921-1935
DOI: 10.1177/0021998315597742

changed only by 5…10% for Weibull shape parameters between 6 and 8. Therefore, the fiber misalignment cannot explain the discrepancy between the Weibull-predicted fiber breakage count and the high frequency AE registrations, and other explanations should be explored.

## 4.2 Simultaneous fiber breakage

The second hypothesis for explaining the discrepancy between the number of Weibull-predicted fiber breaks and the high frequency AE registrations is the possible weakness of an AE event generated by an isolated fiber breakage. It is hypothesized that simultaneous breakage of several fibers is needed to create a noticeable AE event. To evaluate this hypothesis, the model of fiber breakage in a fiber bundle, proposed by Swolfs et al. is used. This model has been extensively described in literature[16-20,30]. This description will not be repeated here, but the main points and input parameters will be highlighted.

The model considers an impregnated bundle of parallel fibers. Unfortunately, due to high computational costs, it is impossible to model the full specimen size studied in the experiments. Instead, a single 6K yarn with a 10 mm length was modelled. In the model, each fiber is divided into fiber elements with a length of 3.5 µm, giving a total of 2857 elements per fiber. A strength value is assigned to each element according to the Weibull distribution. The applied longitudinal strain on the bundle of fibers is gradually incremented. At each strain increment, fiber failure is checked by comparing element stress with element strength. If a fiber element fails, then this element locally loses its load transfer capability and the stress on the nearby fiber elements increases. This stress redistribution is taken into account by the model using the finite element (FE) data in literature[16, 17]. Fiber element failure is then checked again until no new elements break within the same strain increment. If no new element failures are detected, then the model increments the strain. This is repeated until final failure is detected.

The procedure allows the groups of fiber breaks to be tracked. Two fiber breaks are part of the same group if (1) the lateral distance between their fiber centers is smaller than 4 fiber radiuses, and (2) the axial distance between both breaks is less than 10 fiber radiuses. This definition corresponds to the dimensions of the zone where the stress concentrations are significant. Simultaneous fiber breakage is defined as two or more fiber breaks that fail within the same strain increment and are part of the same group of fiber breaks.

The model parameters were chosen in such a way that they can represent the fiber bundles in both 2D and 3D materials in an average way. The axial fiber stiffness was 230 GPa, and the full engineering constants for the fibers can be found in Swolfs et al.[30]. The matrix stiffness was 3 GPa. The fiber volume fraction was 70%, which corresponds to the measured fiber volume fractions inside yarns[25]. The Weibull distribution $P_f$ is used to assign a strength value to each fiber element[29]:

Journal of Composite Materials 50 (2016) p. 1921-1935
DOI: 10.1177/0021998315597742

$$P_f = 1 - \exp\left[ -\left( \frac{L}{L_0} \right) \cdot \left( \frac{\sigma_f}{\sigma_0} \right)^m \right], \tag{5}$$

where $\sigma_f$ is the fiber strength, $\sigma_0$ is the Weibull scale parameters, $L$ is the element length, $L_0$ is the reference gauge length, and $m$ is the Weibull shape parameter or modulus. The Weibull modulus was either 5 or 8, which are typical values for carbon fiber[31]. The Weibull scale parameter was adapted to obtain a composite failure strain of 1.8%, which corresponds to the failure strain from the carbon fiber datasheets. The reference gauge length $L_0$ was 10 mm. A total of 100 simulations were performed for both Weibull moduli, and the number of fiber breaks and groups of fiber breaks were averaged. This average is then multiplied by 612. This factor is obtained from the ratio of the volume of fibers in the warp direction of the 2D weave over the volume of fibers in the strength model. This multiplication factor was chosen because it lies in between the factors 1034 and 571 for the 3D weave in warp and fill direction respectively. If one of these limiting values is chosen, then the results are scaled differently, but their interpretation would remain the same.

Fig. 10 presents the results of the simultaneous fiber breaks and compares it with the cluster analysis results. The results agree reasonably well with the cluster analysis results, especially compared to the discrepancies with the analysis presented in Lomov et al.[5], which roughly corresponds to the "all breaks" curve in Fig. 10. The agreement seems to be better for m=8 than for m=5. While this does not prove that AE is unable to detect single fiber breaks, it does shed a new light on what AE can detect. For the total number of fiber breaks, the cluster analysis results yield much lower values than the Weibull prediction. This discrepancy exists despite existing evidence of a one-to-one correlation between the number of AE events and the number of fiber breaks observed by the polarized light microscope in the single fiber tensile test[26, 32]. Further experimental work is needed to confirm that AE indeed only detects simultaneous fiber breaks in fiber-reinforced polymer composites.

Journal of Composite Materials 50 (2016) p. 1921-1935
DOI: 10.1177/0021998315597742

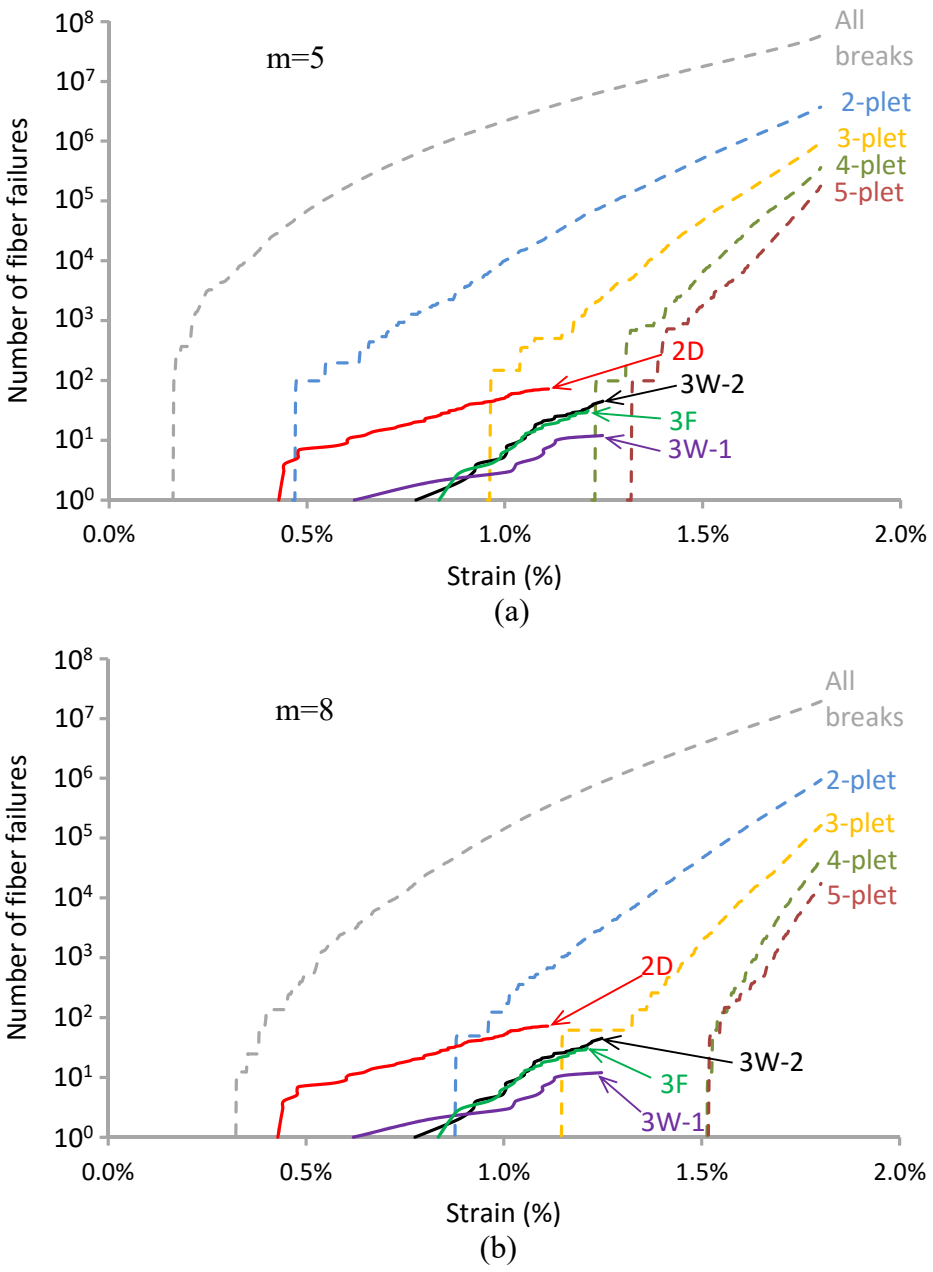


**Fig. 10: Comparison between the number of high frequency AE events and the average number of grouped fiber failures that occurred simultaneously in the strength model: (a) for a Weibull modulus of 5, and (b) for a Weibull modulus of 8. An i-plet is defined as a group of "i" fiber breaks near each other that fail within the same strain increment. The "All breaks" data does not satisfy this definition, but is added nonetheless to facilitate comparison.**

## 5. Conclusions

In this study, unsupervised cluster analysis is performed for AE registration of 2D and 3D carbon/epoxy woven composites during tension loading. Peak amplitude and

frequency features were found to be the most relevant for the cluster analysis. Different frequency features were however found to be crucial for different specimens. For example, the peak frequency was the most relevant frequency feature for 2D woven, while this was the frequency centroid for 3D woven composites. Therefore it is advisable to perform a full cluster analysis to achieve a reliable classification of the AE events.

The AE cluster structure for carbon/epoxy woven composites is the same as for their previously studied[21] glass/epoxy counterparts. The only difference is that the cluster bounds of amplitude and frequency for the carbon/epoxy composites are higher than for the glass/epoxy.

The development of high frequency AE events under increasing tensile loading and predictions of simultaneous fiber breakage based on Weibull statistics were compared. This comparison suggested that the AE events in the high frequency cluster correspond to the simultaneous breakage of fibers in the bundles. This gives additional grounds for the hypothesis that high frequency AE events represent fiber breakage.

## Acknowledgments

The research visit of L. Li to KU Leuven was funded by Chinese Scholarship Council and partially supported by FWO project G.0354.09. The raw AE data used in the present study and damage images in Fig. 1 were acquired by M. Karahan[4] and N. De Greef[3]. The authors thank the Agency for Innovation by Science and Technology in Flanders (IWT) for a grant given to Y. Swolfs. The authors are grateful to L. Gorbatikh for the discussion of the presented results.

The X-ray computed tomography images have been made on the X-ray computed tomography facilities at the KU Leuven, financed by the Hercules Foundation (project AKUL 09/001: Micro- and nano-CT for the hierarchical analysis of materials), and maintained under supervision of Prof M. Wevers. The authors would like to thank A.E. Bogdanovich (NCSU, USA) for the provision of the material and for useful discussions of the material's internal structure. The help with Vallen AE system of Johan Vanhulst and useful discussions with Dr. Sergey Ivanov are acknowledged with gratitude.

## References

1. Bourchak M, Farrow I, Bond I, Rowland C and Menan F. Acoustic emission energy as a fatigue damage parameter for CFRP composites. *Int J Fatigue* 2007; 29: 457-470.
2. Bourchak M, Khan A, Badr SA and Harasani W. Acoustic emission characterization of matrix damage initiation in woven CFRP composites. *Mater Sci Appl* 2013; 4: 509-515.
3. De Greef N, Gorbatikh L, Godara A, Mezzo L, Lomov SV and Verpoest I. The effect of carbon nanotubes on the damage development in carbon fiber/epoxy composites. *Carbon* 2011; 49: 4650-4664.
4. Bogdanovich AE, Karahan M, Lomov SV and Verpoest I. Quasi-static tensile behavior and damage of carbon/epoxy composite reinforced with 3D non-crimp orthogonal woven fabric. *Mech Mater* 2013; 62: 14-31.

5. Lomov S, Karahan M, Bogdanovich A and Verpoest I. Monitoring of acoustic emission damage during tensile loading of 3D woven carbon/epoxy composites. *Text Res J* 2014; 84: 1373-1384.
6. Karimi NZ, Minak G and Kianfar P. Analysis of damage mechanisms in drilling of composite materials by acoustic emission. *Compos Struct* 2015; 131: 107-114.
7. Fotouhi M, Saeedifar M, Sadeghi S, Najafabadi MA, and Minak G. Investigation of the damage mechanisms for mode I delamination growth in foam core sandwich composites using acoustic emission. *Struct Health Monit* 2015; 14: 265-280.
8. Lomov SV, Ivanov D, Truong T, et al. Experimental methodology of study of damage initiation and development in textile composites in uniaxial tensile test. *Compos Sci Technol* 2008; 68: 2340-2349.
9. Sause M, Gribov A, Unwin A and Horn S. Pattern recognition approach to identify natural clusters of acoustic emission signals. *Pattern Recogn Lett* 2012; 33: 17-23.
10. Sause M, Müller T, Horoschenkoff A and Horn S. Quantification of failure mechanisms in mode-I loading of fiber reinforced plastics utilizing acoustic emission analysis. *Compos Sci Technol* 2012; 72: 167-174.
11. Gutkin R, Green C, Vangrattanachai S, Pinho S, Robinson P and Curtis P. On acoustic emission for failure investigation in CFRP: Pattern recognition and peak frequency analyses. *Mech Syst Signal Pr* 2011; 25: 1393-1407.
12. Valentin D, Bonniau P and Bunsell A. Failure mechanism discrimination in carbon fibre-reinforced epoxy composites. *Compos* 1983; 14: 345-351.
13. Liu P, Chu J, Liu Y and Zheng J. A study on the failure mechanisms of carbon fiber/epoxy composite laminates using acoustic emission. *Mater Design* 2012; 37: 228-235.
14. Berthelot J and Rhazi J. Acoustic emission in carbon fibre composites. *Compos Sci Technol* 1990; 37: 411-428.
15. De Groot PJ, Wijnen PA and Janssen RB. Real-time frequency determination of acoustic emission for different fracture mechanisms in carbon/epoxy composites. *Compos Sci Technol* 1995; 55: 405-412.
16. Swolfs Y, Gorbatikh L, Romanov V, Orlova S, Lomov SV and Verpoest I. Stress concentrations in an impregnated fibre bundle with random fibre packing. *Compos Sci Technol* 2013; 74: 113-120.
17. Swolfs Y, Gorbatikh L and Verpoest I. Stress concentrations in hybrid unidirectional fibre-reinforced composites with random fibre packings. *Compos Sci Technol* 2013; 85: 10-16.
18. Swolfs Y, McMeeking R, Verpoest I, Gorbatikh L. Matrix cracks around fibre breaks and their effect on stress redistribution and failure development in unidirectional composites. *Compos Sci Technol* 2015; 108:16-22.
19. Swolfs Y, McMeeking R, Verpoest I, Gorbatikh L. Initial failure development in unidirectional hybrid composites revealed through modelling. *Compos Part A: Appl S* 2014; 69: 279-287.
20. Swolfs Y, Morton H, Scott AE, Gorbatikh L, Reed PAS, Sinclair I. Synchrotron radiation computed tomography for experimental validation of a tensile strength model for unidirectional fibre-reinforced composites. *Compos Part A: Appl S* 2014; DOI: 10.1016/j.compositesa.2015.06.018.

21. Li L, Lomov SV, Yan X and Carvelli V. Cluster analysis of acoustic emission signals for 2D and 3D woven glass/epoxy composites. *Compos Struct* 2014; 116: 286–299.
22. Maillet E, Baker C, Morscher GN, Pujar VV, and Lemanski JR. Feasibility and limitations of damage identification in composite materials using acoustic emission. *Compos Part A: Appl S* 2015; 75: 77-83.
23. Ono K and Cho H. Experimental transfer functions of practical acoustic emisssion sensors. In: *28 European Conference of AE Testing*, Cracow UT, 2008, pp. 25-30.
24. He X, Cai D and Niyogi P. Laplacian score for feature selection. *Advances in neural information processing systems*. Vancouver, BC, Canada, 5 - 8 December, 2005, pp. 507-514.
25. Jolliffe I. Principal component analysis. *Wiley Online Library*, 2005.
26. Karahan M, Lomov SV, Bogdanovich AE, Mungalov D and Verpoest I. Internal geometry evaluation of non-crimp 3D orthogonal woven carbon fabric composite. *Compos Part A: Appl S* 2010; 41: 1301-1311.
27. Giordano M, Calabro A, Esposito C, D'Amore A and Nicolais L. An acoustic-emission characterization of the failure modes in polymer-composite materials. *Compos Sci Technol* 1998; 58: 1923-1928.
28. Straumit I, Lomov, S.V. Wevers, M. Quantification of the internal structure and the automatic generation of voxel models of textile composites from X-ray computed tomography data. *Compos Part A: Appl S* 2015; 69:150-158.
29. Swolfs Y, Verpoest I and Gorbatikh L. Issues in strength models for unidirectional fibre-reinforced composites. *Compos Sci Technol* 2015; 114: 42-49.
30. Swolfs Y, Gorbatikh L, Romanov V, Orlova S, Lomov SV and Verpoest I. Stress concentrations in an impregnated fibre bundle with random fibre packing. *Compos Sci Technol* 2013; 74: 113-120.
31. Naito K. Tensile properties of polyacrylonitrile- and pitch-based hybrid carbon fiber/polyimide composites with some nanoparticles in the matrix. *J Mater Sci Lett* 2013; 48: 4163-4176.
32. Godin N, Huguet S, Gaertner R and Salmon L. Clustering of acoustic emission signals collected during tensile tests on unidirectional glass/polyester composite using supervised and unsupervised classifiers. *NDT & E Int* 2004; 37: 253-264.